Scaling in necklaces of monopoles and semipoles

Mark Hindmarsh[*]

Department of Physics and Astronomy, University of Sussex, Falmer, Brighton BN1 9QH, United Kingdom
and Department of Physics and Helsinki Institute of Physics, P.O. Box 64,
FI-00014 University of Helsinki, Finland

Anna Kormu,[†] Asier Lopez-Eiguren,[‡] and David J. Weir[§]

Department of Physics and Helsinki Institute of Physics, P.O. Box 64,
FI-00014 University of Helsinki, Finland

Models of symmetry breaking in the early universe can produce networks of cosmic strings threading 't Hooft-Polyakov monopoles. In certain cases there is a larger global symmetry group and the monopoles split into so-called semipoles. These networks are all known as cosmic necklaces. We carry out large-scale field theory simulations of the simplest model containing these objects, confirming that the energy density of networks of cosmic necklaces approaches scaling, i.e., that it remains a constant fraction of the background energy density. The number of monopoles per unit comoving string length is constant, meaning that the density fraction of monopoles decreases with time. Where the necklaces carry semipoles rather than monopoles, we perform the first simulations large enough to demonstrate that they also maintain a constant number per unit comoving string length. We also compare our results to a number of analytical models of cosmic necklaces, finding that none explains our results. We put forward evidence that annihilation of poles on the strings is controlled by a diffusive process, a possibility not considered before. The observational constraints derived in our previous work for necklaces with monopoles can now be safely applied to those with semipoles as well.

I. INTRODUCTION

Symmetry-breaking phase transitions in the early universe are a natural consequence of attempts to explain physics beyond the standard model, for example by incorporating the elements of the standard model in a grand unified theory (GUT). Depending on the nature of the symmetry that is broken during such a phase transition, it is possible for topological defects to have formed. Defects are solitonic solutions of the field equations carrying conserved topological charge; however, the word is used more loosely to mean any extended classical structures in the field, including long-wavelength Goldstone modes.

In cosmology the most interesting defects are cosmic strings [1] (see Refs. [2–5] for reviews). They appear even in the simplest case of the Abelian Higgs model, forming when the U(1) gauge symmetry breaks. The cosmic strings arising from this symmetry breaking are Nielsen-Olesen vortex lines [6]. Similar objects can also arise as fundamental objects in an underlying string theory.

These objects, termed F- and D-strings, are also known as cosmic superstrings [7–11].

More complex patterns of symmetry-breaking or models with extra dimensions can produce structures which are combinations of different kinds of defect. Models of this type that have attracted attention in recent years include semilocal strings [12–16], which are a combination of Goldstone modes and cosmic strings; necklaces [17–23], which are a combination of strings and monopoles; and related models where the monopoles form string junctions [24,25]. The first direct numerical simulations of necklace networks were performed by some of the authors of this article in Ref. [26].

In this paper we continue our investigation of the non-Abelian strings started in Ref. [26]. The particular theory with which we work models, in its most basic form, a two-stage GUT symmetry-breaking scenario where first an SU(2) symmetry breaks to a U(1), forming 't Hooft-Polyakov monopoles. Later, at a lower symmetry-breaking scale, this U(1) itself breaks in a manner analogous to that in the simpler Abelian Higgs model. The result is that the magnetic flux of the 't Hooft-Polyakov monopoles is then carried by two cosmic string segments linking the monopoles together. This, then, spontaneously breaks a Z_2

[*]m.b.hindmarsh@sussex.ac.uk
[†]anna.kormu@helsinki.fi
[‡]asier.lopezeiguren@helsinki.fi
[§]david.weir@helsinki.fi

symmetry that relates the magnetic charge of the monopoles and the orientation of the strings.

A monopole that is attached to two cosmic strings in this way is termed a "bead" and a system of many such beads on a loop of string forms a "necklace." As shown in Ref. [23] the beads can be seen as the kinks form when $Z_2 \times Z_2$ symmetry is spontaneously broken to Z_2 by the string solutions. An exact solution is known in a model with $\mathcal{N} = 2$ supersymmetry [20].

When the symmetry-breaking scales are degenerate, the global symmetry $Z_2 \times Z_2$ is enlarged to D_4, the square symmetry group. When D_4 breaks down to Z_2, the kinks that are formed are labeled by a Z_4 topological charge and they can be seen as split beads. That is, each bead separates into two "semipoles." Semipoles can annihilate only with the corresponding antisemipole. Unlike monopoles, two adjacent semipoles need not have total charge zero, and they can repel each other [23]. We will refer to monopoles and semipoles collectively as "poles." Semipoles come in two different types, depending on a ratio of dimensionless couplings λ and κ in the scalar potential [23]. In Ref. [26] we simulated only with $\kappa/2\lambda \geq 1$; here, we perform the first simulations for $\kappa/2\lambda < 1$. We do not revisit the special case $\kappa/2\lambda = 1$, where the symmetry group on the string is enhanced to $O(2)$ and semipoles do not exist.

In order to characterize the gross features of a network of cosmic necklaces we can use two length scales: the average comoving pole separation, ξ_m, and the average comoving string separation, ξ_s. These quantities are of great interest for the analysis of the network evolution because they show if the system has reached scaling. Scaling is an important property for the reliable study of defect networks, because it tells us how to extrapolate network observables to large cosmic times. Scaling, in its simplest form as applied to cosmic string networks, means that all quantities with dimensions of length grow in proportion to the horizon distance, $\xi \propto \tau$. In a scaling string network, the fraction of the energy density coming from defects remains constant. However, necklaces have an important dynamical length scale [19]

$$d_{\mathrm{BV}} = \frac{M_m}{\mu}, \qquad (1)$$

where M_m is the monopole mass and μ the string mass per unit length.[1] The inverse $1/d_{\mathrm{BV}}$ sets the scale for the acceleration of a monopole attached to a bent string. For strings alone, the local acceleration is equal to the curvature, so there is no fixed scale in the dynamics. This is the underlying reason for why strings approach scaling. One cannot apply the same argument to necklaces, and their scaling is more difficult to understand.

It turns out to be informative to study the linear comoving monopole density

$$n = \frac{\xi_s^2}{\xi_m^3}, \qquad (2)$$

or equivalently the linear physical monopole density in units of d_{BV} [19],

$$r = d_{\mathrm{BV}} n/a, \qquad (3)$$

where a is the cosmological scale factor.

The mean comoving energy density of the network is

$$\rho_n \simeq \frac{\mu}{\xi_s^2}(1 + r), \qquad (4)$$

from which one can see that r is the string-to-monopole mean energy density ratio. Therefore, if the strings scale ($\xi_s \propto \tau$) and r is a constant, the network will maintain a constant density fraction.

One would expect that when $r \ll 1$ the string evolves essentially without regard to the poles. On the other hand, when r is significant the evolution of the network should change in some way.

Firmly establishing the behavior of r, or equivalently n, is important for predictions of observable signals from necklaces, including the production of high energy cosmic rays, cosmic microwave background fluctuations, and gravitational waves.

In Ref. [19], it was suggested that the density of monopoles on strings would grow to be so large as to dominate the dynamics. This would slow the string network down, leading to large numbers of monopole-antimonopole annihilation events and a copious source of ultrahigh energy cosmic rays.

On the other hand, Ref. [27] argued that monopoles acquire substantial velocities along the string, similar in magnitude to the transverse velocities of the strings themselves, leading to frequent monopole interaction events on the string, and efficient monopole annihilation. The number of monopoles per unit length should therefore decrease toward the minimum allowed by causality $1/t$, and the strings should end up behaving like an ordinary cosmic string network, with RMS velocity a significant fraction of the speed of light.

In Ref. [28] the velocity-dependent one-scale model was adapted to necklace models, with the principal conclusion being that both ξ_s and ξ_m should be expected to scale in most circumstances, and that the monopole velocities are driven towards unity, with continuously increasing Lorentz factors.

With contradictory results from analytical studies, direct numerical simulations are required. In Ref. [26], we carried out the first field-theory simulations of the system, but with restricted dynamic range the conclusions we could draw were rather limited. Evidence was presented that the monopole-necklace system evolves towards a state with a linear increase in the comoving string separation ξ_s with conformal time and

---

[1]The mass of a monopole or semipole on a string is generally less than that of a free pole, but still the same order of magnitude.

r tending to zero in such a way that n remained approximately constant. In the semipole case, n appeared to increase toward the end of the simulations. The behavior was not definitively established as the simulations were not large enough. In all cases, the energy density of the necklaces was transferred efficiently to propagating modes of the gauge and scalar fields, much as for Abelian Higgs cosmic strings [29], implying that necklaces are not an important source of gravitational waves.

In the present paper we go beyond these earlier simulations, and establish firmly the scaling properties of the network. We are able to analyze larger mass ratios than before. We also explore the effect of different defect separations in the initial conditions.

We are able to reject important hypotheses made in the previous model-building attempts outlined above, in particular: the monopole-to-string density ratio r never increases, in contradiction with the Berezinky-Vilenkin model [19]; the decrease is slower than $r \propto t^{-1}$, in contradiction with the Blanco-Pillado and Olum model [27]; and the monopole velocities asymptote to a constant value, in contradiction with the Martins model [28].

We confirm that the monopoles pick up a substantial component of velocity along the string [27]. We also confirm the findings of Ref. [26] that the scaling state for the string-monopole system has a linear increase in the comoving string separation ξ_s with conformal time, and constant comoving linear monopole density n.

For necklaces with semipoles we find similar behavior, independent of the parameter ratio $\kappa/2\lambda$ which controls their type: like necklaces with monopoles, both the RMS velocity and the comoving linear density n tend to a constant.

We have been unable to produce a satisfactory model that explains the observed monopole and semipole densities. The fact that the monopole density decreases more slowly than envisaged in the model of Blanco-Pillado and Olum means that monopole annihilation is not as efficient as proposed, but we have not been able to establish why. We put forward a proposal based on pole diffusion in the Discussion.

The paper is organized as follows: In Secs. II and III we describe the model and the numerical simulations. Then in Sec. IV we show the results obtained and in Sec. V we compare them to necklace evolution models. Finally, in Sec. VI we discuss the results obtained.

II. MODEL

The model that we study is the SU(2) Georgi-Glasgow model with two Higgs fields in a spatially flat Robertson-Walker metric. In this section we will introduce the model and summarize its most important aspects. A more detailed description of the model can be found in Refs. [17,23].

In comoving coordinates x^i, conformal time $\tau = x^0$, and with scale factor a, the action is

$$\mathcal{S} = \int d^4x \left(-\frac{1}{4} F_{\mu\nu}^a F^{\mu\nu a} + a^2 \sum_n \text{Tr}[D_\mu, \Phi_n][D^\mu, \Phi_n] \right.$$
$$\left. - a^4 V(\Phi_1, \Phi_2) \right), \tag{5}$$

where $D_\mu = \partial_\mu + igA_\mu$ is the covariant derivative, $A_\mu = A_\mu^a \sigma^a/2$, and σ^a are Pauli matrices. The Higgs fields Φ_n, $n = 1, 2$, are in the adjoint representation, $\Phi_n = \phi_n^a \sigma^a/2$. Spacetime indices have been raised with the Minkowski metric with mostly negative signature.

The potential can be written in the following way:

$$V(\Phi_1, \Phi_2) = -m_1^2 \text{Tr}\Phi_1^2 - m_2^2 \text{Tr}\Phi_2^2$$
$$+ \lambda(\text{Tr}\Phi_1^2)^2 + \lambda(\text{Tr}\Phi_2^2)^2 + \kappa(\text{Tr}\Phi_1\Phi_2)^2, \tag{6}$$

where λ and κ are positive and $m_{1,2}$ are real.

The system undergoes two symmetry-breaking phase transitions, $\text{SU}(2) \to \text{U}(1) \to Z_2$. After the first symmetry-breaking the theory has 't Hooft-Polyakov monopole solutions and after the second one the theory has string solutions. The vacuum expectation values of the two adjoint scalar fields are given by $\text{Tr}\Phi_{1,2}^2 = m_{1,2}^2/2\lambda$, where the scalar masses are then $\sqrt{2}m_{1,2}$. Without loss of generality we will take that Φ_1 has the larger vacuum expectation value, that is, it is the responsible field for the first symmetry-breaking.

Depending on the value of the parameters of the potential, m_1, m_2, λ and κ, the model can accommodate three different kinds of solutions, see Ref. [23]:

(i) When $m_1^2 > m_2^2$ the system has a discrete global $Z_2 \times Z_2$ symmetry under which $\Phi_1 \to \pm\Phi_1$ and $\Phi_2 \to \pm\Phi_2$. The string solutions break $Z_2 \times Z_2$ to Z_2 and the resulting kinks are the beads that interpolate between two string solutions. This solutions can be interpreted as 't Hooft-Polyakov monopoles with their flux confined to two tubes.

(ii) When $m_1^2 = m_2^2$ the system has a square symmetry D_4 which is broken to Z_2 by strings. The resulting kinks can be seen as beads that are split into two. Each one of these kinks are known as semipoles. Semipoles can only be annihilated with the corresponding antisemipole. Two classes of solutions exist according to whether $\kappa/2\lambda < 1$ or $\kappa/2\lambda > 1$.

(iii) When $m_1^2 = m_2^2$ and $\kappa/2\lambda = 1$ there is a global O(2) symmetry. This symmetry is spontaneously broken by the string solution but not the vacuum. In this case there are no semipoles and the strings carry persistent global currents. We do not investigate this case here.

III. SIMULATION DETAILS

A. Numerical setup

We discretize the system on a comoving 3D spatial lattice with lattice spacing of $dx = 1$ and time-step of

$d\tau = 0.1$. Then, the lattice equations of motion are evolved using the standard leapfrog method. We perform 1920^3 simulations in the radiation dominated era, for which $a \propto \tau^\nu$ with $\nu = 1$. More information about the discretization and simulation details can be found in Ref. [26].

Analysis of observables should be done once the system has reached scaling, so that extrapolation to cosmologically relevant times is possible. To reduce uncertainties, we want scaling to be reached over as large a time interval as possible, and this can be achieved by choosing a good set of initial conditions. The aim is to generate a random distribution of well-separated defects with otherwise minimal field excitations, consistent with the field configuration expected at a large time after the phase transition. The details of the phase transition itself are not important for the late-time field configuration.

In our case we choose $\Phi_{1,2}$ to have uniformly distributed random values in the range $[-0.5, 0.5]$ for each component $\phi_{1,2}^a$, which we then normalize to the vev of the field in question. The SU(2) gauge field is set up by generating a random SU(2) matrix from four Gaussian random numbers u^0, u^a which are normalized to obtain a unitary matrix of determinant 1.

Once the initial field configuration is set we smooth the configuration of the Higgs fields, that is, in each lattice point we substitute the field value by a weighted average of the field values at the actual lattice point and at the six nearest neighbors:

$$\Phi_n(\mathbf{x}) \to \frac{1}{12} \sum_i [\Phi_n(\mathbf{x} - \hat{\imath}) + 2\Phi_n(\mathbf{x}) + \Phi_n(\mathbf{x} + \hat{\imath})]. \quad (7)$$

We apply this smoothing N_s times to the initial configuration, a number which is in general different for the two fields. The aim of this differential smoothing is to explore networks with different initial densities of monopoles and strings, allowing us to vary n.

After smoothing the initial configuration we run with relatively strong damping period for a time $\delta\tau_d$. The damping term is handled using the Crank-Nicolson method [30], but is rather stronger than adopted in Ref. [26]; we take $\sigma = 4$ in the notation of that paper.

The heavy damping phase ends at $\tau = 120$, after which we run the simulation with the standard Hubble damping for one light-crossing time of the box, at which point conformal time is $\tau_{\text{end}} = 2040$.

As with all simulations in fixed comoving volume in an expanding background, physical widths such as the size of the defects shrink, which presents a two-fold problem: to make sure they are well-separated in the beginning and well-resolved at the end. A common approach in field theory simulations of this type is to scale the couplings and mass parameters with factors a^{1-s}, where a is the cosmological scale factor and $0 \leq s \leq 1$. This procedure keeps the scalar expectation values fixed and the string tension constant but the comoving width of the string core grows

for $s < 1$. In our simulations we use $s = 1$, but we run with $s = -1$ from the end of the damping period until time τ_{cg}. This means that the comoving width of the string can be made small while they are formed. It also accelerates the production of the network, because the conformal time taken by the fields to settle to their vacua is of the order the comoving defect width. The scale factor is normalized to $a(\tau_{\text{end}}) = 1$, so that the defects remain resolved throughout the simulation.

In principle, correlations can start to be established after half a light-crossing time. However, the only massless excitations are waves on the string, and the strings are much longer than the box size even at the end of the simulations. We therefore do not expect finite-size effects, although we check for small deviations from scaling toward the end of the simulations.

B. Measurements

During the simulation we measure the number of poles N and the string length L. In order to obtain the monopole number we compute the magnetic charge in each lattice site. The string length is computed by counting the plaquettes pierced by strings, that is, counting the plaquettes with a gauge-invariant "winding" in the U(1) subgroups formed by projection with the scalar field Φ_1, the heavier one in the nondegenerate case.

In the case of monopoles, this measurement process gives the magnetic field $\mathbf{B}^{(1)}$ and, by calculating the divergence, the exact number of monopoles. For semipoles with $\kappa/2\lambda < 1$, this yields approximately half the semipoles; the rest are sources or sinks of a magnetic field $\mathbf{B}^{(2)}$ obtained by projecting out the U(1) gauge field associated with Φ_2 [23]. Finally, when $\kappa/2\lambda > 1$, the relevant magnetic fields are $\mathbf{B}^{(\pm)} = (\mathbf{B}^{(1)} \pm \mathbf{B}^{(2)})/\sqrt{2}$, and our measurement of $\mathbf{B}^{(1)}$ sources and sinks picks out features in the field configuration of a string rather than the semipoles themselves. We call these midpoints "pseudopoles."

On the other hand, the measurements of the winding number—and hence the string length and velocity—do not depend on the particular choice of projecting scalar field. See the Appendix of Ref. [26] for details of the projectors used.

Figure 1 shows a snapshot of the end of one of the semipole simulations (the next-to-last in Table I), with the strings in black and the semipoles represented by red and blue circles.

Using the pole number N, and the string length L we can derive the average comoving defect separations as

$$\xi_{\text{m}} = (V/N)^{1/3}, \qquad \xi_{\text{s}} = (V/L)^{1/2}, \qquad (8)$$

from which we calculate the linear comoving pole density [Eq. (2)] and r [Eq. (3)]. As explained above, the quantity N for semipoles and pseudopoles counts only half the total number, but we retain the definition as it is more directly comparable with the number of monopoles.
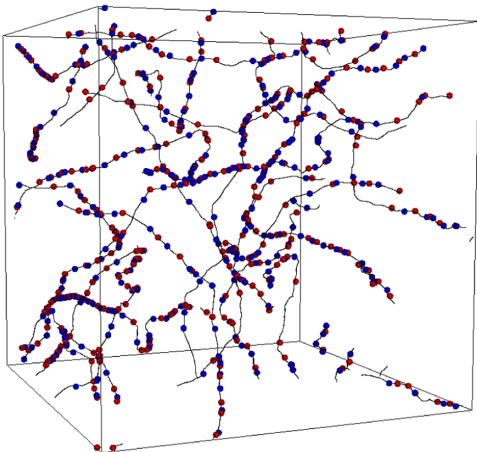
FIG. 1. Snapshot of a semipole necklace at the end of the simulation. The black lines represent the strings, the red circles the poles picked out by $\mathbf{B}^{(+)}$ and the blue circles the poles picked out by $\mathbf{B}^{(-)}$. The run parameters are given in the last entry of Table I.

We use the positions of the strings and poles to compute the string root-mean-square (RMS) velocity $\bar{v}_s$, and the monopole RMS velocity $\bar{v}_m$. Once we have the positions of poles and strings at each time step we can follow their trajectories during the simulation. Computing the trajectory at every time step $d\tau$ is computationally very expensive, and it can also induce some noise due to lattice discretization ambiguities. Therefore, we perform the computations to obtain the trajectories every time interval $\delta\tau_v = 20d\tau$.

We also record global quantities such as the total energy and pressure, from which energy conservation can be checked. In all runs global covariant energy conservation is maintained to 1% or better. Detailed information about the measurements can be found in Ref. [26].

C. Parameter choices

We analyse the cases with degenerate ($m_1^2 = m_2^2$) and nondegenerate mass parameters, which allows us to study both monopoles (discrete global $Z_2 \times Z_2$ symmetry) and semipoles (square D_4 symmetry). In the semipole case we analyse two different parameter relations, $\kappa/2\lambda > 1$ and (for the first time) $\kappa/2\lambda < 1$.

For monopoles, we explore various ratios of m_1^2 to m_2^2 and various initial configurations, that is, different values for the smoothing iterations, N_s and different damping periods $\delta\tau_d$. More precisely, all the runs are carried out with $m_1^2 = 0.25$ in the radiation-dominated era ($\nu = 1$) and the scale factor is normalized so that $a = 1$ at the end of the simulations.

The values of the rest of the parameters can be seen in Table I. We perform one realization for each set of parameter choices.

IV. RESULTS

A. Length scales

The comoving necklace network length scales ξ_s and ξ_m, which are defined in Eq. (8) are plotted in Figs. 2 and 3. In these plots we show all the cases for which we have carried out simulations.

The effect of the different amounts of smoothing in the initial conditions can bee seen in the initial defect separations: the more smoothing, the further apart the defects. The amount of damping makes little difference to the initial defect separation, but does reduce the oscillations in the RMS deviation of the field from its vacuum value, $\delta\Phi_{1,2} = |\mathrm{Tr}\Phi_{1,2}^2 - v_{1,2}^2|^{1/2}$. The subsequent evolution depends little on the initial conditions: the system evolves toward a scaling regime characterized by $\xi_s \propto \tau$.

In order to analyze the scaling regime we have computed the gradients for the comoving string separation ξ_s, in three different time regimes. These time ranges, which are $\tau \in [1000, 1250]$, $\tau \in [1250, 1500]$ and $\tau \in [1500, 1750]$, are chosen to cover the biggest part of the dynamical range taking into account that the system needs some time to reach scaling after the core growth period. The values of the gradients can be seen in Table II. The gradients confirm that

TABLE I. List of simulation parameters for the runs we performed. The dimensionful parameters are given in units of the lattice spacing dx. Potential parameters (6) are shown along with the isolated monopole mass M_m and the isolated string tension μ. The length scale $d_{BV} = M_m/\mu$ is also shown as well as the smoothing iterations $N_s(\Phi_1)/N_s(\Phi_2)$, damping time $\delta\tau_d$ and end of the core growth period in conformal time, τ_{cg}, and physical time, t_{cg}. Simulations were run until conformal time $\tau = 2040$.

| m_1^2	m_2^2	λ	κ	M_m	μ	d_{BV}	N_s	$\delta\tau_d$	τ_{cg}	t_{cg}
0.25	0.1	0.5	1	11	0.63	17.5	10000/10000	350	520	66
0.25	0.1	0.5	1	11	0.63	17.5	4000/10000	350	520	66
0.25	0.1	0.5	1	11	0.63	17.5	1000/10000	350	520	66
0.25	0.1	0.5	1	11	0.63	17.5	4000/10000	87.5	520	66
0.25	0.025	0.5	1	11	0.16	70	4000/4000	350	520	66
0.25	0.0125	0.5	1	11	0.08	140	4000/4000	350	520	66
0.25	0.25	0.5	0.25	11	1.6	7	4000/4000	350	520	66
0.25	0.25	0.5	0.5	11	1.6	7	4000/4000	350	520	66
0.25	0.25	0.5	2	11	1.6	7	4000/4000	350	520	66
0.25	0.25	0.5	4	11	1.6	7	4000/4000	350	520	66
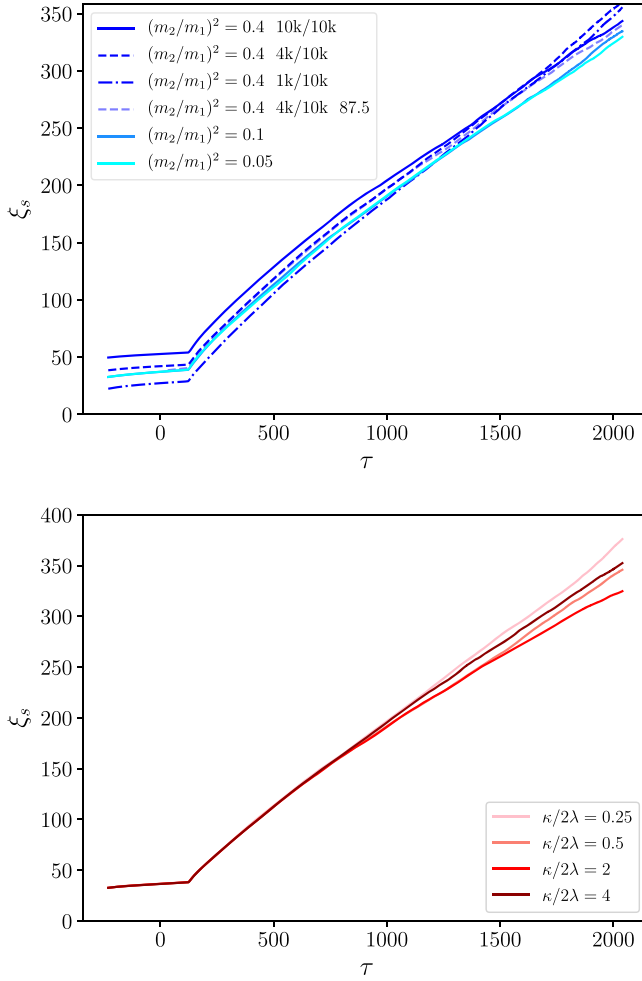
FIG. 2. Mean string separation ξ_s, defined in Eq. (8), for necklaces with monopoles (top) and semipoles (bottom), against conformal time τ. The legend gives the ratio mass-squared values of the fields $(m_2/m_1)^2$ for the necklaces with monopoles and the ratio of scalar couplings $\kappa/2\lambda$ for the necklaces with semipoles. In the case where the mass-squared ratio is 0.4 the legend also shows the number of smoothing steps performed in each field as $N_s(\Phi_1)/N_s(\Phi_2)$. We distinguish the case with the equal amount of smoothing showing the damping time $\delta\tau_d$ where it is the shortest. A full list of simulation parameters is given in Table I.

the strings are indeed scaling. In addition, we can conclude that the finite-size effects are negligible, because the values of the gradients at the final time range are compatible with the values at the other two time ranges.

Analyzing the comoving monopole separation, ξ_m, we can see that it increases slower than τ. However, it keeps increasing during the whole evolution of the system, showing that N decreases and that pole-antipole annihilations are present in all the stages of the evolution.

B. Linear pole density

We can characterize the linear pole density (the number of poles of a particular type per unit length of string) in two
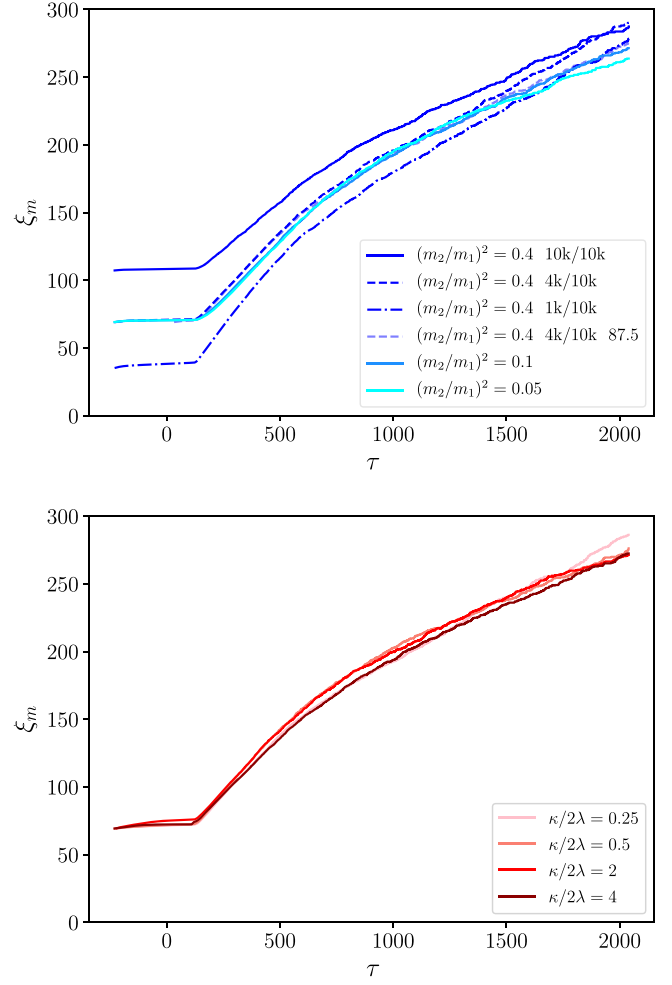
FIG. 3. Mean monopole separation ξ_m, defined in Eq. (4), for necklaces with monopoles (top) and semipoles (bottom), against conformal time τ. See the caption to Fig. 2 for an explanation of the legend.

TABLE II. Results of the ξ_s gradients computed in three different ranges. Numerical annotations refer to the range in which the gradient is computed: 1 has $\tau \in [1000, 1250]$, 2 has $\tau \in [1250, 1500]$ and 3 has $\tau \in [1500, 1750]$. The last two columns are the mean value and the standard deviation computed using the values from the three different regions.

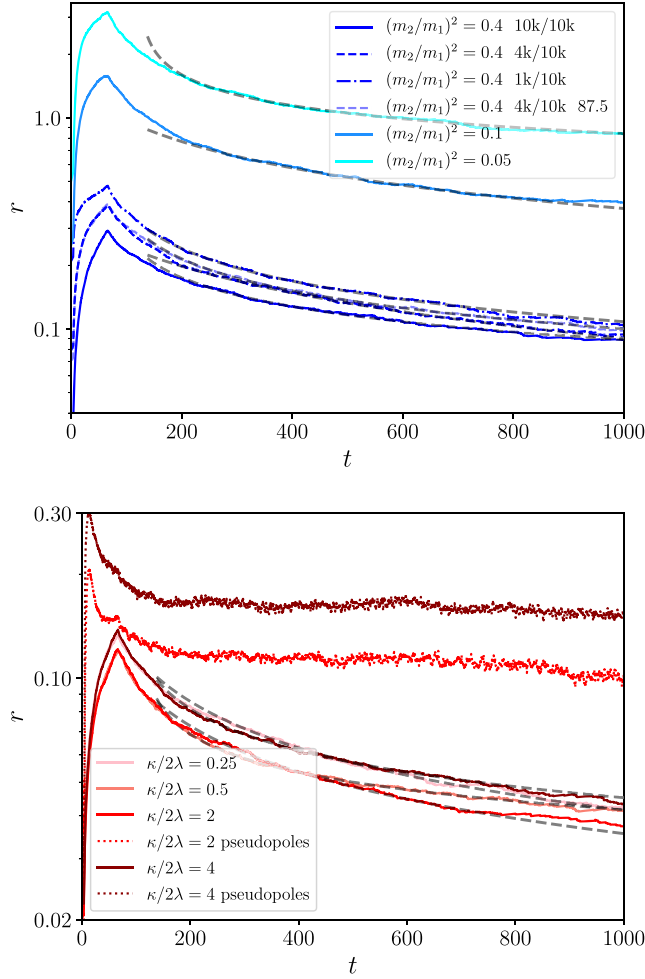| m_2^2/m_1^2	$\kappa/2\lambda$	$\left(\frac{d\xi_s}{d\tau}\right)_1$	$\left(\frac{d\xi_s}{d\tau}\right)_2$	$\left(\frac{d\xi_s}{d\tau}\right)_3$	Mean	Std
0.4	1	0.131	0.140	0.138	0.136	0.005
0.4	1	0.147	0.153	0.152	0.151	0.003
0.4	1	0.154	0.162	0.151	0.156	0.006
0.4	1	0.134	0.155	0.135	0.141	0.012
0.1	1	0.139	0.132	0.134	0.135	0.004
0.05	1	0.140	0.134	0.125	0.133	0.008
1	0.25	0.167	0.166	0.156	0.163	0.006
1	0.5	0.136	0.148	0.162	0.149	0.013
1	2	0.139	0.140	0.127	0.135	0.007
1	4	0.157	0.154	0.151	0.154	0.003

FIG. 4. Linear pole density r (3) for necklaces with monopoles (top) and semipoles (bottom), plotted against physical time t. The dashed grey line represents the fit to the data using the function presented in Eq. (10). The values for the fit parameters can be seen in Table III. See the caption to Fig. 2 for an explanation of the legend. Note that in the plot for necklaces with semipoles we show also the linear pseudopole density in the cases where $\kappa/2\lambda > 1$.

different ways: r, the number per unit physical length in units of the pole acceleration scale $1/d_{\mathrm{BV}}$ (3), and n, the number per comoving string length.

The ratio of pole to string energy density, r, is plotted in Fig. 4 against physical time, which for the radiation dominated era is

$$t = \frac{1}{2}a(\tau)\tau. \tag{9}$$

All the different cases simulated can be found in these figures. We can see that in all the cases the value of r does not increase, once the physical evolution begins at τ_{cg}.

Also plotted is the number per unit physical length of pseudopoles. In this case, r seems to asymptote to a

TABLE III. Parameters computed from fitting r in the range $t \in [245, 750]$ using the function presented in Eq. (10). The uncertainties for β and r_b are obtained using the variations in the values for the four necklace cases with the same physical parameters. However, the uncertainties for t_0 are obtained from the fitting because the value for t_0 can vary in simulations with the same physical parameters but different initial conditions.

m_2^2/m_1^2	$\kappa/2\lambda$	β	r_b	t_0
0.4	1	0.36 ± 0.15	0.10 ± 0.01	60 ± 3
0.4	1	0.70 ± 0.15	0.11 ± 0.01	-184 ± 7
0.4	1	0.46 ± 0.15	0.12 ± 0.01	28 ± 3
0.4	1	0.42 ± 0.15	0.11 ± 0.01	47 ± 3
0.1	1	0.57 ± 0.15	0.43 ± 0.01	-98 ± 7
0.05	1	0.27 ± 0.15	0.92 ± 0.01	122 ± 3
1	0.25	0.46 ± 0.15	0.05 ± 0.01	-6 ± 5
1	0.5	0.22 ± 0.15	0.04 ± 0.01	106 ± 2
1	2	0.46 ± 0.15	0.04 ± 0.01	-9 ± 4
1	4	0.30 ± 0.15	0.05 ± 0.01	68 ± 3

constant of order 10^{-1}, indicating a constant physical separation along the string. Although there is no extra energy density associated with a pseudopole, it does suggest that there is a physical length scale on the string of around $10d_{\mathrm{BV}}$ imprinted in the fields.

In order to analyze the power law with which r decreases we fit with the following function:

$$r = r_b[(t - t_0)/(t_b - t_0)]^{-\beta}, \tag{10}$$

where r_b, t_0 and β are the fitting parameters and we choose t_b to be the end of the fitting range $[t_a, t_b] = [245, 750]$. The values of the fitting parameters can be found in Table III.

The fits indicate that r decreases with a power law close to $t^{-1/2}$, which would indicate that the comoving density $n = ar/d_{BV}$ should be approximately constant. In Fig. 5 we can see that for n does indeed appear to tend to a constant at large time, consistent with the results in Ref. [26].

The asymptotic values of n at large conformal time are about a factor of 2 smaller than in our previous simulations, which has no particular physical significance. Instead, we note that the behavior $r \propto t^{-1/2}$ brings in a new length scale D, which can be defined from

$$r = \frac{d_{\mathrm{BV}}}{\sqrt{2Dt}}. \tag{11}$$

Using the value of n at the last time step of the simulation one can obtain an approximate value for D. As we have already noted, all the cases seem to asymptote to the same value of n, so we can extract an estimate of a universal D by taking the average over all the realizations. The value computed is $D = 16 \pm 2$.

The results for n for semipoles in Ref. [26] were not conclusive, and we now understand that in using the source
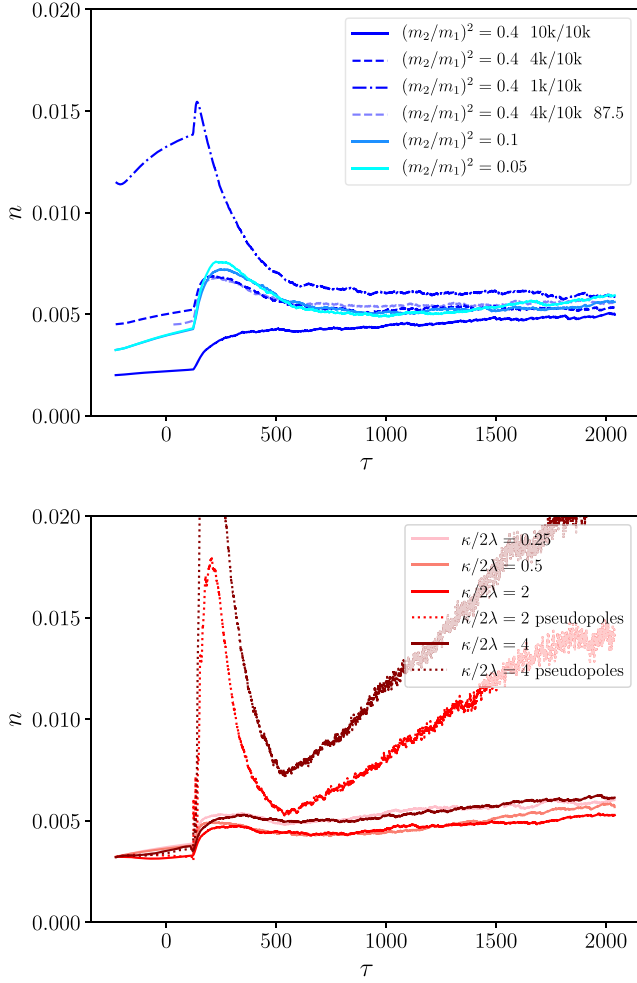
FIG. 5. The number of poles per comoving string length n for the necklaces with monopoles (top) and semipoles (bottom), plotted against conformal time τ; in the semipole case only one type of semipoles ($\mathbf{B}^{(1)}$ or $\mathbf{B}^{(+)}$) is shown. See the caption to Fig. 2 for an explanation of the legend. Note that in the plot for necklaces with semipoles, we show also the number of $\mathbf{B}^{(1)}$ pseudopoles per comoving string length in the cases where $\kappa/2\lambda > 1$.
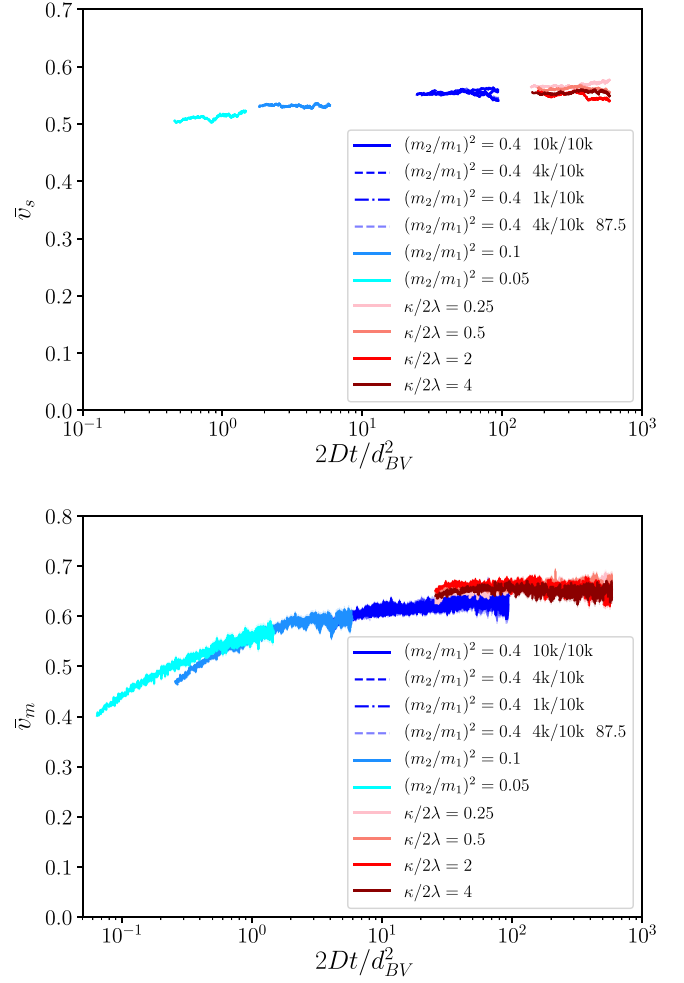
FIG. 6. The root mean square velocity for strings (top) and monopoles (bottom) computed by the method outlined in Sec. III B, plotted against $2Dt/d_{BV}^2$, where t is physical time, d_{BV} is the acceleration time scale (1), and D is the length scale defined from Eq. (11). The average values for the velocities can be found in Table IV. See the caption to Fig. 2 for an explanation of the legend.

of $\mathbf{B}^{(1)}$ flux to locate the semipoles was incorrect. Our new results for semipoles establish that they behave in the same way as monopoles.

The linear density of the sources of $\mathbf{B}^{(1)}$ flux (pseudopoles) is nonetheless instructive. We have therefore also plotted the pseudopole separation in Figs. 4 and 5, for which r asymptotes to $O(10^{-1})$, and n increases linearly with conformal time, as expected for an asymptotically constant r.

C. Velocities

In Fig. 6, we show the RMS velocities computed for strings and poles using the procedure described in Sec. III B, plotted against physical time in units of $d_{\mathrm{BV}}^2/2D$. The velocities in different simulations fall on an approximately consistent curve which appears to asymptote to a constant at large times. Semipoles move faster (see Table IV). The curve

TABLE IV. Values of the velocities of the strings and poles and the pole velocity relative to the string. The velocities are computed in $t \in [297, 900]$. The error shown is the standard deviation obtained from averaging over all the timesteps.

m_2^2/m_1^2	$\kappa/2\lambda$	$\bar{v}_s$	$\bar{v}_m$	$\bar{v}_{\mathrm{rel}}$
0.4	1	0.552 ± 0.005	0.63 ± 0.01	0.30 ± 0.05
0.4	1	0.558 ± 0.003	0.629 ± 0.009	0.29 ± 0.04
0.4	1	0.555 ± 0.002	0.629 ± 0.008	0.30 ± 0.04
0.4	1	0.553 ± 0.004	0.63 ± 0.01	0.29 ± 0.04
0.1	1	0.532 ± 0.002	0.592 ± 0.008	0.26 ± 0.04
0.05	1	0.513 ± 0.005	0.56 ± 0.01	0.21 ± 0.07
1	0.25	0.568 ± 0.004	0.658 ± 0.009	0.33 ± 0.04
1	0.5	0.561 ± 0.002	0.660 ± 0.009	0.35 ± 0.03
1	2	0.549 ± 0.002	0.652 ± 0.008	0.35 ± 0.03
1	4	0.555 ± 0.002	0.648 ± 0.008	0.33 ± 0.03

is particularly noticeable for the light strings, which need more time to accelerate the monopoles to their asymptotic speed. RMS velocity values can be seen in Table IV.

One can obtain an estimate of the velocities of the monopoles and semipoles along the string using the string and pole RMS velocities $\bar{v}_{\mathrm{rel}}^2 = \bar{v}_{\mathrm{m}}^2 - \bar{v}_{\mathrm{s}}^2$, also given in Table IV. Note that $\bar{v}_{\mathrm{rel}}^2 \sim \bar{v}_{\mathrm{s}}^2$ in all cases, with larger relative velocities for semipoles. In our previous simulations we were unable to measure the RMS velocities well enough to gain an unambiguous nonzero value for the motion of the poles along the strings.

V. COMPARISON TO NECKLACE EVOLUTION MODELS

Having presented the results of our simulations, we compare our findings to the analytical models presented in the literature. The models all make assumptions about the system, and derive various predictions, which differ between models. We can test the validity of the assumptions and the correctness of the predictions in light of our new results.

The first model describing the evolution of the necklace network was introduced by Berezinsky and Vilenkin (BV) in Ref. [19]. The authors assumed that there is no motion of monopoles along the strings and that monopole-antimonopole annihilation is negligible. They also argued that the typical velocity of the strings and monopoles was

$$\bar{v}_{\mathrm{s}} \sim \frac{1}{\sqrt{1+r}}, \tag{12}$$

based on considering the necklace to have an effective mass per unit length $\mu_{\mathrm{eff}} = \mu + M_{\mathrm{m}}N/aL$, while maintaining tension μ. They presented the following differential equation for r, in the regime where $r \ll 1$:

$$\frac{\dot{r}}{r} = -\frac{\kappa_s}{t} + \frac{\kappa_g}{t}. \tag{13}$$

The first term on the right-hand side describes string stretching due to the expansion of the Universe, and has $\kappa_s = \gamma(1 - 2\bar{v}_{\mathrm{s}}^2)$, where $\gamma = t\dot{a}/a = \nu/(1+\nu)$. The second one models the competing effect of strings shrinking due to energy loss, with $\kappa_g \simeq 1$. In Ref. [19] the primary energy loss channel was thought to be gravitational radiation, but the field radiation observed in the numerical simulations of topological defects (see also Ref. [29]) will also have the same effect.

Using the string velocities obtained in our work and the estimated value for κ_g from Ref. [19], the solution to Eq. (13) has r growing with a power of time close to 1. Their conclusion was therefore that if r is initially small, it will grow.

Our results show the contrary: r decreases in all the cases that we considered (see Fig. 4). Our simulations show that the number of monopoles N decreases during the evolution
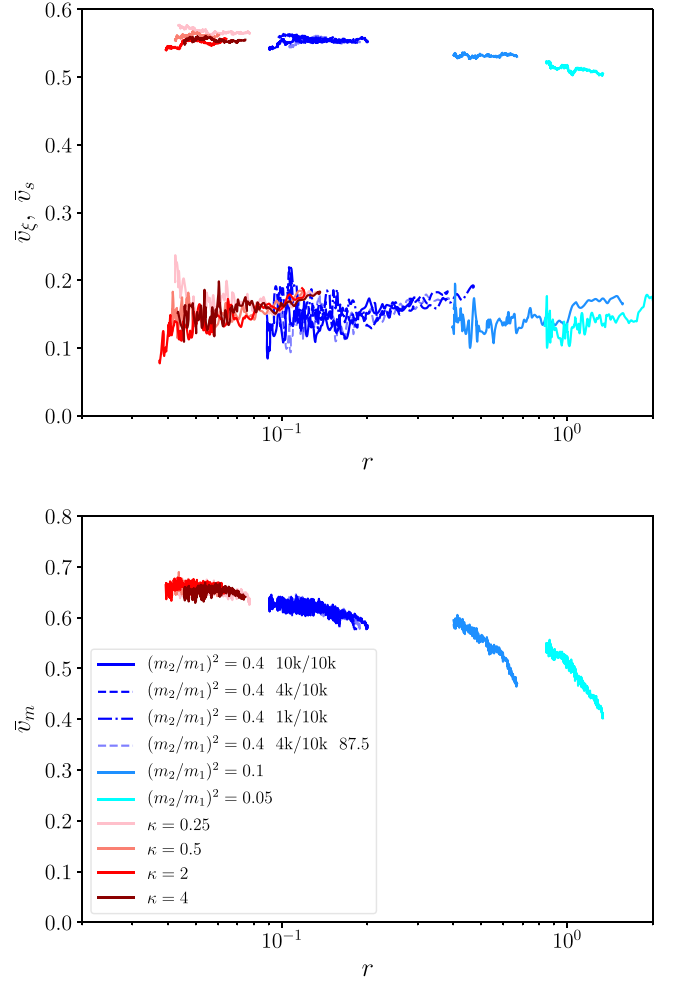

FIG. 7. Plots showing the RMS string velocity $\bar{v}_s$ against r (top) and $\bar{v}_m$ against r (bottom). In the top plot we have also included data showing $\bar{v}_\xi = d\xi_s/d\tau$ against r, where the $\bar{v}_\xi$ data is smoothed over a Blackman window with 101 points. See the caption to Fig. 2 for an explanation of the legend, which is the same in both plots.

of the system, demonstrating that monopole-antimonopole annihilations are important. Animations of network evolution (See Refs. [31–33]) indicate that annihilations take place both on long strings and loops.

Another major difference with Ref. [19] is in the dependence of the string velocity on r. In Fig. 7 (top) we have plotted the directly computed $\bar{v}_s$ against r. The gradient of the mean string separation $d\xi_s/d\tau$ has dimensions of velocity, and provides an estimate of the string RMS velocity on the scale ξ_s, which we denote $\bar{v}_\xi$. We have therefore also plotted $\bar{v}_\xi$, smoothed with a Blackman filter over 101 time steps, which is clearly distinguished by having much smaller values.

It is clear that there is no evidence for a dependence of the large-scale velocity $\bar{v}_\xi$ on r. The short-distance measure $\bar{v}_s$ decreases very slightly for $r \simeq 1$, but certainly not by a factor $1/\sqrt{2}$ as predicted by Eq. (12).

The directly computed monopole RMS velocity $\bar{v}_{\rm m}$ is shown in Fig. 7 (bottom). There is some evidence for a slow decrease of the monopole RMS velocity with increasing r, which is probably due to the correlation between higher r and earlier times, before the monopoles have picked up full speed. By eye, there is some suggestion that there is a common asymptote of $\bar{v}_{\rm m} \simeq 0.7$ as $r \to 0$, which is the long-time limit of the necklace evolution.

Monopole annihilation is incorporated into the model of Blanco-Pillado and Olum [27]. They also used the BV assumption for the string velocities (12), but argued that there should be approximate equipartition between the components of the monopole and string RMS velocities, and therefore the RMS velocity component of monopoles along the strings should be

$$\bar{v}_{\rm rel}^2 \simeq \bar{v}_{\rm s}^2/2. \tag{14}$$

They concluded that there should be frequent encounters between monopoles and antimonopoles on the string, which would result in efficient annihilations. The mean monopole spacing should therefore be of order $t/\bar{v}_{\rm rel}$ (physical units), and hence r should decrease as t^{-1}.

Our results are consistent with approximate velocity equipartition, $\bar{v}_{\rm rel} \sim \bar{v}_{\rm s}$ (see Table IV). However, our results for r are inconsistent with the $r \propto t^{-1}$ behavior predicted in Ref. [27]. For monopoles and semipoles, the fits to a power law are closer to $r \propto t^{-1/2}$, consistent with constant comoving linear density n. (See Table III).

The third model is a velocity-dependent one-scale model for monopoles [34] adapted for the evolution of necklaces [28]. This model focuses on the evolution of the separation between monopoles, assuming that the string velocity obeys Eq. (12) and that the mean string separation is similar to the mean monopole separation,

$$\xi_{\rm m} \sim \xi_{\rm s}. \tag{15}$$

With these assumptions for the strings, it should be sufficient to study the mean separation and RMS velocity of the monopoles, and the evolution equations for these parameters were derived to be (in our notation)

$$3\frac{d\xi_{\rm m}}{dt} = (3 + \bar{v}_{\rm m}^2)H\xi_{\rm m} + Q_*, \tag{16}$$

$$\frac{d\bar{v}_{\rm m}}{dt} = (1 - \bar{v}_{\rm m}^2)\left(\frac{k_s}{d_{\rm BV}} - H\bar{v}_{\rm m}\right), \tag{17}$$

where H is the Hubble parameter, k_s the phenomenological string curvature parameter [35,36] and Q_* a constant energy loss term.

The solution of Eqs. (16), (17) has $\xi_{\rm m} \propto t$ and $\bar{v}_{\rm m} \to 1$. This describes an evolution where $r \propto t^{-1}$ and the monopoles' Lorentz factor continually increases with time. Again,

this disagrees with our results, which indicate that $r \propto t^{-1/2}$ and $\bar{v}_{\rm m} \simeq 0.6$.

In conclusion, we can say that none of the models of which we are aware describes our results: the key difference is the behavior of r, the linear physical monopole density in units of $d_{\rm BV}$. The physical linear density decreases—in contradiction to the BV model—as a result of monopole annihilation. However, the monopole annihilation cannot be as efficient as assumed in the other two models, as r decreases in proportion to $t^{-1/2}$ rather than t^{-1}. Semipoles behave like monopoles.

VI. DISCUSSION

We have carried out the largest simulations to date of systems of necklaces, studying both monopoles and semipoles, exploring a wider range of string-to-monopole energy density ratios r than before, and following the evolution to larger string separations.

Our results concern the mean comoving string separation $\xi_{\rm s}$, the mean comoving monopole (or semipole) separation $\xi_{\rm m}$, the mean RMS string velocity $\bar{v}_{\rm s}$, and the mean RMS monopole velocity $\bar{v}_{\rm m}$.

The mean comoving string separation $\xi_{\rm s}$ always increases with conformal time, consistent with linear scaling $\xi_{\rm s} \propto \tau$. The slopes are shown in Table II. The mean separation of monopoles and semipoles, grows as $\xi_{\rm m} \propto \tau^{2/3}$. The rest have r decreasing in proportion to $t^{-1/2}$, equivalent to a a constant comoving linear density n (see Fig. 5). In terms of the physical mean separation and physical time, $\xi_{\rm m}^{\rm phy} \propto t^{5/6}$.

String RMS velocities tend to a constant value $\bar{v}_{\rm s} \simeq 0.55$, only weakly dependent on the string-to-monopole energy density ratio r.

Monopole and semipole RMS velocities evolve slowly toward a constant value around 0.7 at the end of our simulations, on a timescale controlled by the monopole acceleration parameter $1/d_{\rm BV}$. The RMS velocities in the limit of vanishing string-to-monopole energy density ratio r appear to be tending to a common value around 0.7.

Models of necklace evolution in the literature do not describe our results. A key point is that the assumed dependence of the RMS string velocity on the monopole-to-string density ratio r (12) is not observed. Instead, the RMS string velocity barely depends on r at all, up to $r \simeq 2$. Thus the picture of massive monopoles as slowing down the strings is incorrect; instead, it seems that the strings can drag the monopoles around with them, although the more massive the monopoles, the longer it takes for their RMS velocity to reach that of the strings.

Monopole and semipole annihilation is certainly important, contrary to [19], but has much lower efficiency than envisaged in Ref. [27], who argued that monopoles would annihilate with probability of order unity if they encountered each other on the string. If the poles have an RMS

velocity along the string of $\bar{v}_{\parallel}$, the average pole should encounter others at a conformal time rate $\bar{v}_{\parallel} n$. Thus if σ is the annihilation probability, we should be able to write a one-dimensional Boltzmann equation

$$\frac{dn}{d\tau} = n\left(-\sigma\bar{v}_{\parallel}n + 2\frac{1}{\xi_s}\frac{d\xi_s}{d\tau}\right), \tag{18}$$

where the second term on the right hand side describes the increase in the comoving linear density due to the string shrinking. It seems reasonable at first sight to identify $\bar{v}_{\parallel}$ with $\bar{v}_{\rm rel}$, and assuming constant σ, this equation would have a solution $n = \nu_0/\tau$, with $\nu_0 = 3/\sigma\bar{v}_{\rm rel}$. This is equivalent to $r \propto t^{-1}$, and is essentially the model put forward in Ref. [27]. The fact that n appears to tend to a constant is inconsistent with the model, and therefore at least one of the assumptions that go into it. Either there is some mechanism suppressing annihilation, or it is incorrect to make the identification $\bar{v}_{\parallel} \sim \bar{v}_{\rm rel}$.

The constraint that semipoles can annihilate only with a corresponding antisemipole does not appear to significantly change their annihilation rate in comparison to monopoles.

We do not have a clear idea of how the suppression of pole annihilation happens, despite their appreciable short-distance motion along the string, $\bar{v}_{\rm rel} \simeq 0.3$. One possibility is that $\bar{v}_{\rm rel}$ is a short-distance measure of velocity, while $\bar{v}_{\parallel}$ is effectively averaged over a scale d, the average comoving separation of poles along the string. This measure of velocity could decrease as τ^{-1} if the pole motion were more like diffusion than uniform linear translation. Perhaps short distance fluctuations on the string, analogous to the Lüscher term on the QCD string [37], act to keep the monopoles in some kind of Brownian motion.

As explained earlier, $r \propto t^{-1/2}$ brings in a new length scale D, which can be defined from $r = d_{\rm BV}/\sqrt{2Dt}$, indicating that the RMS linear separation between poles is $\sqrt{2Dt}$. This could be explained by the poles executing Brownian motion, with diffusion constant $D \simeq 16$ in lattice units, and annihilating with O(1) probability when meeting. The average velocity on the pole separation scale would go as $\sqrt{2D/t}$, proportional to τ^{-1} as required for the constant

n solution to (18). We do not have a good microscopic explanation for the value of D, although we note an order-of-magnitude coincidence with the separation of pseudo-poles, sources of a certain U(1) flux not associated with a local increase of energy density. Significant computer time would be required to investigate pole annihilation further.

In summary, we have found strong evidence that the necklace network as a whole scales, in the sense that its energy density remains a constant fraction of the total energy density, now for semipoles as well as monopoles [26]. The fractional energy density of poles decreases as $t^{-1/2}$, suggesting a diffusive process. The energy in the necklaces is lost to radiative modes of the gauge and scalar fields.

The cosmological implications of this kind of scaling necklace network were discussed in Ref. [26]; in summary, the principal observational constraints come from diffuse γ-rays for necklaces in a sector with substantial couplings to the standard model ($G\mu \lesssim 3 \times 10^{-11}$) or the cosmic microwave background for necklaces in a hidden sector ($G\mu \lesssim 10^{-7}$).

[1] T. Kibble, J. Phys. A **9**, 1387 (1976).

[2] M. Hindmarsh and T. Kibble, Rep. Prog. Phys. **58**, 477 (1995).

[3] A. Vilenkin and E. P. S. Shellard, *Cosmic Strings and Other Topological Defects* (Cambridge University Press, Cambridge, England, 2000).

[4] E. J. Copeland, L. Pogosian, and T. Vachaspati, Classical Quantum Gravity **28**, 204009 (2011).

[5] M. Hindmarsh, Prog. Theor. Phys. Suppl. **190**, 197 (2011).

[6] H. B. Nielsen and P. Olesen, Nucl. Phys. **B61**, 45 (1973).

[7] E. Witten, Phys. Lett. **153B**, 243 (1985).

[8] S. Sarangi and S. H. Tye, Phys. Lett. B **536**, 185 (2002).

[9] E. J. Copeland, R. C. Myers, and J. Polchinski, J. High Energy Phys. 06 (2004) 013.

[10] J. Urrestilla and A. Vilenkin, J. High Energy Phys. 02 (2008) 037.

[11] J. Lizarraga and J. Urrestilla, J. Cosmol. Astropart. Phys. 04 (2016) 053.

[12] T. Vachaspati and A. Achúcarro, Phys. Rev. D **44**, 3067 (1991).

[13] A. Achucarro and T. Vachaspati, Phys. Rep. **327**, 347 (2000).

[14] A. Achucarro, P. Salmi, and J. Urrestilla, Phys. Rev. D **75**, 121703 (2007).

[15] A. Achúcarro, A. Avgoustidis, A. M. M. Leite, A. Lopez-Eiguren, C. J. A. P. Martins, A. S. Nunes, and J. Urrestilla, Phys. Rev. D **89**, 063503 (2014).

[16] A. Lopez-Eiguren, J. Urrestilla, A. Achúcarro, A. Avgoustidis, and C. J. A. P. Martins, Phys. Rev. D **96**, 023526 (2017).

[17] M. Hindmarsh and T. Kibble, Phys. Rev. Lett. **55**, 2398 (1985).

[18] M. Aryal and A. E. Everett, Phys. Rev. D **35**, 3105 (1987).

[19] V. Berezinsky and A. Vilenkin, Phys. Rev. Lett. **79**, 5202 (1997).

[20] D. Tong, Phys. Rev. D **69**, 065003 (2004).

[21] Y. Ng, T. W. B. Kibble, and T. Vachaspati, Phys. Rev. D **78**, 046001 (2008).

[22] T. W. B. Kibble and T. Vachaspati, J. Phys. G **42**, 094002 (2015).

[23] M. Hindmarsh, K. Rummukainen, and D. J. Weir, Phys. Rev. Lett. **117**, 251601 (2016).

[24] T. Vachaspati and A. Vilenkin, Phys. Rev. D **35**, 1131 (1987).

[25] M. Hindmarsh and P. Saffin, J. High Energy Phys. 08 (2006) 066.

[26] M. Hindmarsh, K. Rummukainen, and D. J. Weir, Phys. Rev. D **95**, 063520 (2017).

[27] J. J. Blanco-Pillado and K. D. Olum, J. Cosmol. Astropart. Phys. 05 (2010) 014.

[28] C. J. A. P. Martins, Phys. Rev. D **82**, 067301 (2010).

[29] M. Hindmarsh, J. Lizarraga, J. Urrestilla, D. Daverio, and M. Kunz, Phys. Rev. D **96**, 023525 (2017).

[30] J. Crank and P. Nicolson, Adv. Comput. Math. **6**, 207 (1996).

[31] Necklaces with monopoles video, https://vimeo.com/226143102 (2017).

[32] Necklaces with semipoles $\kappa = 0.25$ video, https://vimeo.com/227731826 (2017).

[33] Necklaces with semipoles $\kappa = 2$ video, https://vimeo.com/227731071 (2017).

[34] C. J. A. P. Martins and A. Achucarro, Phys. Rev. D **78**, 083541 (2008).

[35] C. J. A. P. Martins and E. P. S. Shellard, Phys. Rev. D **54**, 2535 (1996).

[36] C. Martins and E. Shellard, Phys. Rev. D **65**, 043514 (2002).

[37] M. Luscher, Nucl. Phys. **B180**, 317 (1981).